Inorg. Chem. **2009**, *48*, 257−266

Facile Conversion of Layered Ruddlesden−Popper-Related Structure Y_2O_3-Doped Sr_2CeO_4 into Fast Oxide Ion-Conducting Fluorite-Type Y_2O_3-Doped CeO_2

Ryan Georg Gerlach, Surinderjit Singh Bhella, and Venkataraman Thangadurai*

University of Calgary, Department of Chemistry, 2500 University Drive NW, Calgary, Alberta, T2N 1N4, Canada

Received September 8, 2008

The present work shows a new solid- and gas-phase reaction technique for the preparation of a fast oxide-ion-conducting Y_2O_3-doped $Ce_{1-x}Y_xO_{2-\delta}$ ($x = 0.1$, 0.2) (YCO), which involves the reaction of layered (Ruddlesden−Popper K_2NiF_4-type) structure Y_2O_3-doped Sr_2CeO_4 (YSCO) with CO_2 at an elevated temperature and subsequent acid-washing. A powder X-ray diffraction study revealed the formation of a single-phase cubic fluorite-type YCO for the CO_2-reacted and subsequent acid-washed product. Energy dispersive X-ray analysis showed the absence of Sr in the CO_2-treated and subsequent acid-washed product, confirming the transformation of layered YSCO into YCO. The cubic lattice constant was found to decrease with increasing Y content in YCO, which is consistent with the other YCO samples reported in the literature. The scanning electron microscopy study showed smaller-sized particles for the product obtained after CO_2- and acid-washed YCO samples, while the high-temperature sintered YCO and the precursor YSCO exhibit larger-sized particles. The bulk ionic conductivity of the present CO_2-capture-method-prepared YCO exhibits about one and half orders of magnitude higher electrical conductivity than that of the undoped CeO_2 and was found to be comparable to those of ceramic- and wet-chemical-method synthesized rare-earth-doped CeO_2.

Introduction

Oxide ion electrolytes are ionic conductors in which the current is carried by the migration of oxide ions through the oxide ion vacancies.[1] They find applications in several solid-state ionic devices such as solid oxide fuel cells (SOFCs), electrolysis, gas sensors (e.g., O_2, H_2, CH_4, etc.), and oxygen pumps.[2−8] Presently, SOFC technology has generated immense interests due to its high efficiency and clean conversion of energy and potential to be powered by a wide variety of fuels (e.g., H_2, NH_3, hydrocarbons, CO). The current SOFC commercialization is mainly based on the conventional fluorite-type Y_2O_3-doped ZrO_2 (YSZ) oxide ion electrolyte, which can be operated in a temperature range of about 800−1000 °C.[2,4,5] The YSZ-based SOFC exhibits several disadvantages that are attributed to the high temperature of operation. They are detrimental as mechanical stress is induced because of different thermal expansion coefficients of the electrolyte and electrodes, interfacial diffusion of Sr and La from the cathode to the electrolyte, a lack of appropriate sealing materials, and a high cost of bipolar separators.[2,3] Therefore, there is a great deal of interest in developing new materials with desired physical, chemical, and mechanical properties for the development of advanced intermediate temperature (IT) SOFCs (500−750 °C).[9−11]

A number of inorganic crystal structures that include perovskites, fluorites, pyrochlores, perovskite-related brownmillerites, layered perovskite (K_2NiF_4-related), and Aurivilius

* Author to whom correspondence should be addressed. Phone: 001 403 210 8649. E-mail: vthangad@ucalgary.ca.

(1) Goodenough, J. B. *Annu. Rev. Mater. Res.* **2003**, *33*, 91–128.
(2) Minh, N. Q. *J. Am. Ceram. Soc.* **1993**, *76*, 563–588.
(3) Carrette, L.; Friedrich, K. A.; Stimming, U. *Fuel Cells* **2001**, *1*, 5–39.
(4) Singhal, S. C. *Solid State Ionics* **2002**, *152−153*, 405–410.
(5) Ormerod, R. M. *Chem. Soc. Rev.* **2003**, *32*, 17–28.
(6) Weber, A.; Ivers-Tiffee, E. *J. Power Sources* **2004**, *127*, 273–283.
(7) Yano, M.; Tomita, A.; Sano, M.; Hibino, T. *Solid State Ionics* **2007**, *177*, 3351–3359.
(8) Ni, M.; Leung, M. K. H.; Leung, D. Y. C. *Int. J. Hydrogen Energy* **2008**, *33*, 2337–2354.
(9) Kendrick, E.; Kendrick, J.; Knight, K. S.; Islam, M. S.; Slater, P. R. *Nat. Mater.* **2007**, *6*, 871–875.
(10) Kuang, X.; Green, M. A.; Niu, H.; Zajdel, P.; Dickinson, C.; Claride, J. B.; Jantsky, L.; Rosseinsky, M. J. *Nat. Mater.* **2008**, *7*, 498–504.
(11) Brett, D. J. L.; Atkinson, A.; Brandon, N. P.; Skinner, S. J. *Chem. Soc. Rev.* **2008**, *37*, 1568–1578.

10.1021/ic801729x CCC: $40.75
Published on Web 12/05/2008

phases and apatites are being considered for the development of fast oxide ion electrolytes with superior functional properties for applications in IT-SOFCs.[12−21] Among them, the fluorite-type structured rare-earth (RE)-doped CeO_2 materials have been investigated as a potential electrolyte for IT-SOFCs.[22−26] For example, Y-, Sm-, and Gd-doped CeO_2 show a bulk oxide ion conductivity of about 10^{-2} S/cm above 500 °C, which is about 15 times higher than that of YSZ at 500 °C and about 4 times higher than that above 750 °C.[22] There are several synthesis methods, including conventional ceramic (solid-state) and soft-chemical methods such as glycine-nitrate,[27] coprecipitation,[28] and polymerization,[29] that are employed to prepare doped ceria electrolytes. These preparation methods play a significant role in determining the microstructure and particle size distributions, which influence the electrical conductivity,[30−33] and particle-size-dependent conductivity was explained using the space charge model.[34,35]

Recently, we have re-examined the chemical stability of Y-doped $BaCeO_3$ in CO_2 at a temperature range of 600−1000 °C.[36] Our investigation was found to be consistent with the literature[37] on the formation of $BaCO_3$ and fluorite-type Y_2O_3-doped CeO_2 (YCO). During the course of our studies toward a further understanding of the formation of fluorite-type doped CeO_2 oxide ion electrolytes from the perovskite-type structure precursors, we have prepared novel *meta-stable* In-doped CeO_2 and Ca+Sm-doped CeO_2 at 800 °C using the new CO_2 capture method.[38] It is pertinent to mention here that our attempt to prepare single-phase In-doped CeO_2 using a ceramic (solid-state) method at elevated temperatures was unsuccessful.[26,38] Unlike $BaCeO_3$,[37a] the Ba-containing double perovskite-like $Ba_3Ca_{1+x}Nb_{2-x}O_{9-\delta}$ (BCN)[37c] and Ta-doped BCN exhibit excellent chemical stability in 100% CO_2 at 800 °C and in boiling water for a long period of time.[39]

With our own continuing interest in understanding the thermodynamic stability of alkaline-earth-containing metal oxides possessing three-dimensional perovksite and layered (two-dimensional) perovskite-related structures in CO_2, we have investigated the chemical and structural stability of a new layered-structure Y_2O_3-doped Sr_2CeO_4 (YSCO). Our work clearly demonstrates the formation of fluorite-type oxide-ion-conducting YCO from the layered perovskite-related YSCO by reaction with CO_2 at an elevated temperature and subsequent acid-washing. The parent Sr_2CeO_4 is a well-known blue-color-emitting phosphore, and its crystal structure and thermodynamic stability have been characterized.[40−43] Also, the present work shows a path for a new precursor route synthesis of doped CeO_2 materials by designing appropriate precursor compounds that are reactive in CO_2 at elevated temperatures.

Experimental Section

Preparation and Characterization. $Sr_2Ce_{0.9}Y_{0.1}O_{3.95}$ and $Sr_2Ce_{0.8}Y_{0.2}O_{3.9}$ were prepared by a conventional ceramic (solid-state) method using stoichiometric amounts of CeO_2 (>99.9% Alfa Aesar), Y_2O_3 (>99.9% Alfa Aesar; dried at 800 °C in the air and cooled to room temperature in a desiccator), and $SrCO_3$ (99% Alfa Aesar) at elevated temperatures in the air. The desired amount of 2-propanol was added to the starting materials in a zirconia bowl and was ball-milled (Pulverisette, Fritsch, Germany) for about 2 h at 150 rotations per minute using zirconia balls. The sample was then taken out of the ball mill, dried in ambient air, and placed in a clean alumina crucible and heated at 800 °C for 12 h. The resultant product was then reground and sintered at 1350 °C for 24 h with a heating and cooling rate of 10 °C per min. In the final stage of heat treatment, the reaction products were pressed into pellets by isostatic pressure. The sintered pellets were crushed into powder for phase characterization employing a powder X-ray diffractometer (PXRD; Bruker D8 powder X-ray diffractometer (Cu Kα, 40 kV, 40 mA)).

(12) Estell, T. H.; Flengas, S. N. *Chem. Rev.* **1970**, *70*, 339–376.
(13) Kendall, K. R.; Navas, C.; Thomas, J. K.; Zur Loye, H. C. *Solid State Ionics* **1995**, *82*, 215–223.
(14) Kendall, R.; Navas, C.; Thomas, J. K.; Zur Loye, H. C. *Chem. Mater.* **1996**, *8*, 642–649.
(15) Inaba, H.; Tagawa, H. *Solid State Ionics* **1996**, *83*, 1–16.
(16) Shuk, P.; Wiemhöfer, H.-D.; Guth, U.¨; Göpel, W.; Greenblatt, M. *Solid State Ionics* **1996**, *89*, 179–196.
(17) Boivin, J. C.; Mairesse, G. *Chem. Mater.* **1998**, *10*, 2870–2888.
(18) Kharton, V. V.; Marques, F. M. B.; Atkinson, A. *Solid State Ionics* **2004**, *174*, 135–145.
(19) Wincewicz, K. C.; Cooper, J. S. *J. Power Sources* **2005**, *140*, 280–296.
(20) Fergus, J. W. *J. Power Sources* **2006**, *162*, 30–40.
(21) Kendrick, E.; Islam, M. S.; Slater, P. R. *J. Mater. Chem.* **2007**, *17*, 3104–3111.
(22) Steele, B. C. H. *Solid State Ionics* **2000**, *129*, 95–110.
(23) Park, S.; Vohs, J. M.; Gorte, R. J. *Nature* **2000**, *404*, 265–266.
(24) Hibino, T.; Hashimoto, A.; Inoue, T.; Tokuno, J. I.; Yoshida, S. I.; Sano, M. *Science* **2000**, *288*, 2031–2033.
(25) Brandon, N. P.; Blake, A.; Corcoran, D.; Cumming, D.; Duckett, A.; El-Koury, K.; Haigh, D.; Kidd, C.; Leah, R.; Lewis, G.; Matthews, C.; Maynard, N.; Oishi, N.; McColm, T.; Trezona, R.; Selcuk, A.; Schmidt, M.; Verdugo, L. *J. Fuel Cell Sci. Technol.* **2004**, *1*, 61–65.
(26) Pearce, M. C.; Thangadurai, V. *Asia-Pacific J. Chem. Eng.* **2008**, in press.
(27) Xia, C.; Liu, M. *Solid State Ionics* **2002**, *152−153*, 423–430.
(28) Ding, D.; Liu, B.; Zhu, Z.; Zhou, S.; Xia, C. *Solid State Ionics* **2008**, *179*, 896–899.
(29) (a) Biswas, M.; Prabhakaran, K.; Gokhale, N. M.; Sharma, S. C. *Mater. Res. Bull.* **2007**, *42*, 609–617. (b) Lu, C.; Worrell, W. L.; Gorte, R. J.; Vohsb, J. M. J. *J. Electrochem. Soc.* **2003**, *150*, A354–A358.
(30) Kosacki, I.; Suzuki, T.; Petrovsky, V.; Anderson, H. U. *Solid State Ionics* **2000**, *136−137*, 1225–1233.
(31) Tschope, A.; Sommer, E.; Birringer, R. *Solid State Ionics* **2001**, *139*, 255–265.
(32) Suzuki, T.; Kosacki, I.; Anderson, H. U. *Solid State Ionics* **2002**, *151*, 111–121.
(33) Surble, S.; Baldinozzi, G.; Dolle, M.; Gosset, D.; Petot, C.; Petot-Ervas, G. *Ionics* **2008**, *14*, 33–36.
(34) Tschope, A. *Solid State Ionics* **2001**, *139*, 267–280.
(35) Tschope, A.; Kilassonia, S.; Briringer, R. *Solid State Ionics* **2004**, *173*, 57–61.
(36) Sneha, S. B.; Thangadurai, V. *J. Solid State Chem.* **2007**, *180*, 2661–266.
(37) (a) Gopalan, S.; Virkar, A. V. *J. Electochem. Soc.* **1993**, *140*, 1060–1065. (b) Tanner, C. W.; Virkar, A. V. *J. Electrochem. Soc.* **1996**, *143*, 1386–1389. (c) Bhide, S. V.; Virkar, A. V. *J. Electrochem. Soc.* **1999**, *146*, 4386–4392. (d) Ryu, K. H.; Haile, S. M. *Solid State Ionics* **1999**, *125*, 355–367. (e) Azad, A. K.; Irvine, J. T. S. *Solid State Ionics* **2007**, *178*, 635–64. (f) Zakowsky, N.; Williamson, S.; Irvine, J. T. S. *Solid State Ionics* **2005**, *176*, 3019–3026. (g) Matsumoto, H.; Kawasaki, Y.; Ito, N.; Enoki, M.; Ishihara, T. *Electrochem. Solid-State Lett.* **2007**, *10*, B77−B80.
(38) Trobec, F.; Thangadurai, V. *Inorg. Chem.* **2008**, *47*, 8972–8984.
(39) Bhella, S. S.; Thangadurai, V. *J. Power Sources* **2008**, DOI: 10.1016/j.jpowsour.2008.09.110.
(40) Danielson, E.; Devenney, M.; Giaquinta, D. M.; Golden, J. H.; Haushalter, R. C.; McFarland, E. W.; Poojary, D. M.; Reaves, C. M.; Weinberg, W. H.; Wu, X. D. *J. Mol. Struct.* **1998**, *470*, 229–235.
(41) Hirai, T.; Kawamura, Y. *J. Phys. Chem. B* **2004**, *108*, 12763–12769.
(42) Shirsat, A. N.; Kaimal, K. N. G.; Bharadwaj, S. R.; Das, D. *Therm. Chim. Acta* **2006**, *447*, 101–105.
(43) Lu, C. H.; Chen, C. T. *J. Sol-Gel. Sci. Technol.* **2007**, *43*, 179–185.

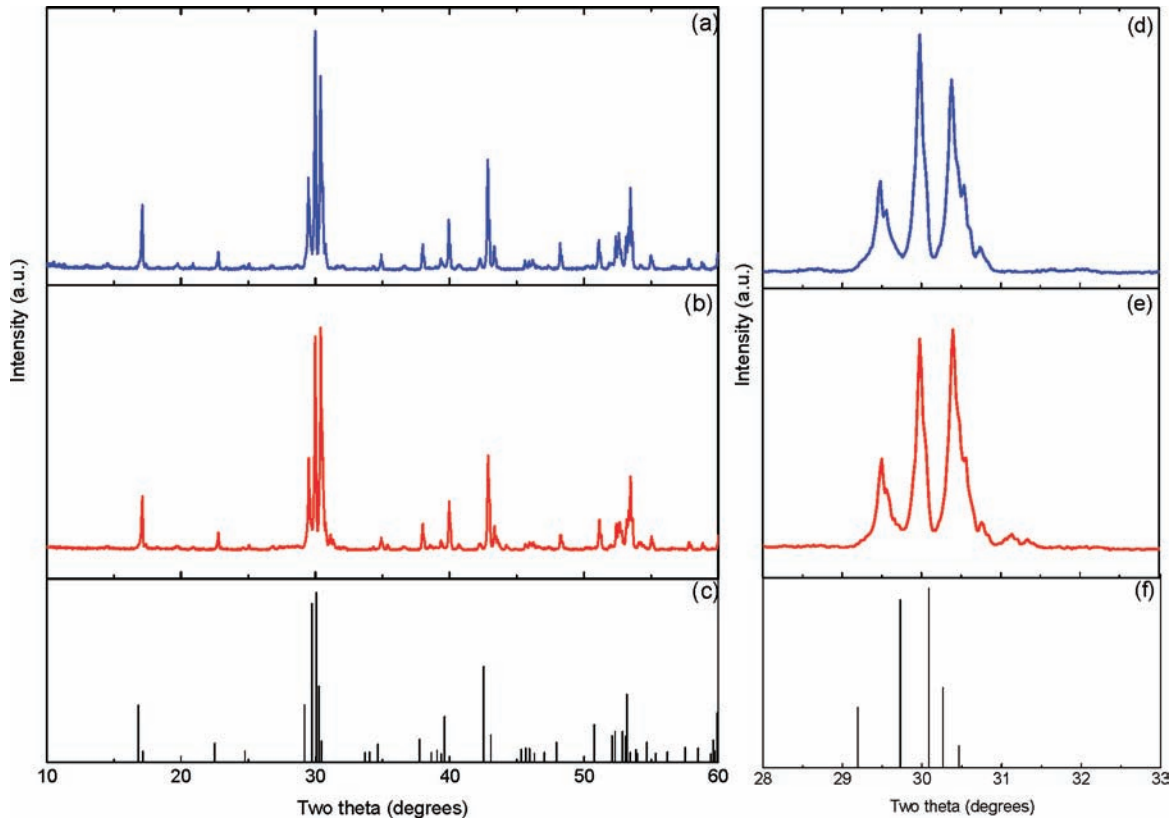

Figure 1. PXRD patterns of (a) $Sr_2Ce_{0.9}Y_{0.1}O_{3.95}$, (b) $Sr_2Ce_{0.8}Y_{0.2}O_{3.9}$ and (c) parent Sr_2CeO_4.[40] Parts d−f show the corresponding selected area PXRD. We see that all of the observed diffraction peaks match well with the expected Sr_2CeO_4 structure.

A known quantity (about 25 g) of YSCO powder was reacted in 100% CO_2 at 600−800 °C for 12 h. After the reaction, the sample was cooled to room temperature (RT) while passing CO_2. The weight gain in the sample was measured using an analytical balance. Then, the resultant product was washed thoroughly using a 1:5 HCl-to-water mixture. Acid was added until stopped CO_2 evolved, and the sample was filtered, washed thoroughly with water, and dried in an ambient atmosphere at RT. The resultant powder sample was characterized using PXRD, scanning electron microscopy (SEM), and energy dispersive X-ray analysis (EDX; Philips XL 30). The lattice constant was determined from PXRD data by least-squares refinement.

Electrical Conductivity Study. Electrical conductivity measurements of the CO_2-capture-method-prepared YCO pellets (∼0.15 cm in thickness and ∼1 cm in diameter) of the acid-washed powder (sintered at 1350 °C for 24 h in an ambient atmosphere) were performed in the air, N_2, and Ar using Pt electrodes (Pt paste obtained from Heraeus Inc., LP A88−11S, Germany, cured at 800 °C in the air for 1 h to remove the organic binders) and employing AC impedance and a gain-phase analyzer (SI model no. 1260; 0.01 Hz to 10 MHz). A two-probe electrochemical cell was used. The applied AC amplitude was 100 mV. Before each electrical measurement, the sample was equilibrated at a constant temperature for at least 1 h. The measurements were made for two subsequent heating and cooling runs.

Results and Discussion

Phase and Microstructure. The PXRD study showed the formation of a single-phase Sr_2CeO_4 structure for all of the investigated YSCO samples. Figure 1 shows the PXRD patterns of $Sr_2Ce_{0.9}Y_{0.1}O_{3.95}$ and $Sr_2Ce_{0.8}Y_{0.2}O_{3.9}$. For comparison, the PXRD data of the parent Sr_2CeO_4 are also included in Figure 1, and it was found that the doped sample shows a similar PXRD pattern.[40,43] Also, we see that Y_2O_3-doped Sr_2CeO_4 samples show a slight shift in the peak position compared to the parent compound. There were no major diffraction peaks observed due to potential impurity in the $SrO-CeO_2-Y_2O_3$ system. It is very interesting to note that the crystal structure of Sr_2CeO_4 has a certain similarity to that of a well-known Ruddlesden−Popper−type (RP) layered structure Sr_2TiO_4 (K_2NiF_4-like).[44,45] In Figure 2, we compare the crystal structures of the parent Sr_2CeO_4 and

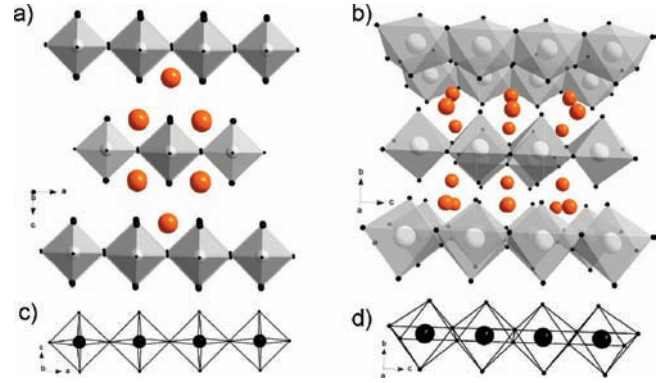

Figure 2. Comparison of crystal structure of Ruddlesdon−Popper (RP) phase K_2NiF_4-related layered Sr_2TiO_4 (a) with structure of Sr_2CeO_4 (b). The balls represent Sr atoms. Parts c and d show the sharing of the single octahedral layers in Sr_2TiO_4 and Sr_2CeO_4, respectively. The octahedral units are edge-shared in Sr_2CeO_4,[40] while they are corner-connected in Sr_2TiO_4.[44,45]

(44) Ruddlesden, S. N.; Popper, P. *Acta Crystallogr.* **1957**, *10*, 538–539.
(45) Ruddlesden, S. N.; Popper, P. *Acta Crystallogr.* **1958**, *11*, 54–55.

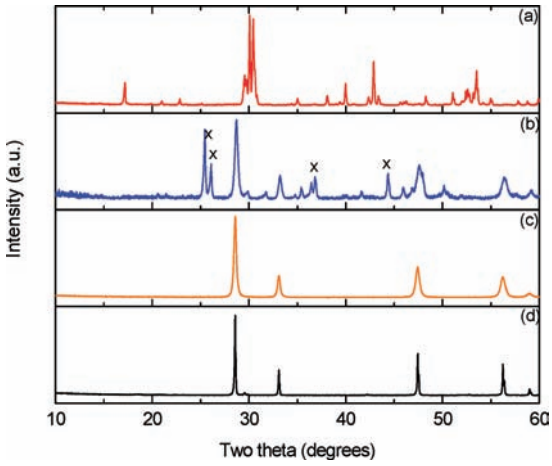

Figure 3. PXRD showing the conversion of K_2NiF_4-related layered structured Y-doped Sr_2CeO_4 into fluorite-type structure 10 mol % Y-doped CeO_2 (a) as-prepared $Sr_2Ce_{0.9}Y_{0.1}O_{3.95}$, (b) sample "a" heated to 800 °C in CO_2 for 12 h, (c) sample "b" washed with dilute acid and subsequently dried in ambient air, and (d) sample "c" sintered at 1350 °C for 24 h in the air. The main diffraction peaks due to $SrCO_3$[46−49] are marked as "x" in b.

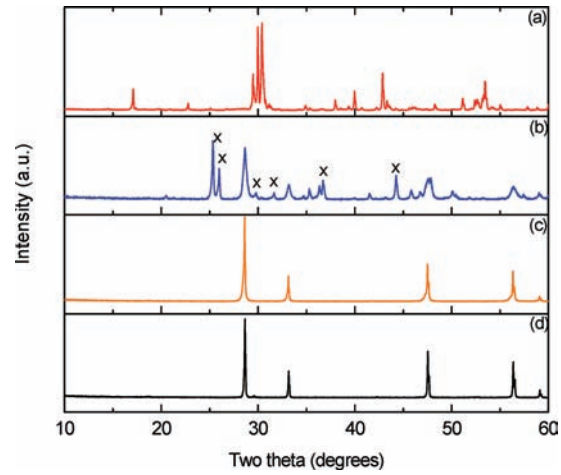

Figure 4. PXRD showing the conversion of K_2NiF_4-related layered Y-doped Sr_2CeO_4 into fluorite-type structure 20 mol % Y-doped CeO_2 (a) as-prepared $Sr_2Ce_{0.8}Y_{0.2}O_{3.9}$, (b) sample "a" heated to 800 °C in CO_2 for 12 h, (c) sample "b" washed with dilute acid and subsequently dried in ambient air, and (d) sample "c" sintered at 1350 °C for 24 h in the air. The main diffraction peaks due to $SrCO_3$[46−49] are marked as "x" in b.

Sr_2TiO_4. The lattice parameters are related as $a_{Sr_2CeO_4} \approx \sqrt{2}a_{Sr_2TiO_4}$; $b_{Sr_2CeO_4} \approx \sqrt{2}a_{Sr_2TiO_4}$, and $c_{Sr_2CeO_4} \approx c_{Sr_2TiO_4}$. Both Sr_2CeO_4 and Sr_2TiO_4 contain MO_6 (M = Ce, Ti) octahedral layers, which are separated by an alkaline layer.[40,43−45] However, the main difference is that in Sr_2CeO_4 the adjacent MO_6 octahedral units are connected via an edge, while in Sr_2TiO_4, they are corner-sharing. The Ce−Ce distance in Sr_2CeO_4 is 3.5 Å,[40,43] which is about 0.5 Å lower than the Ti−Ti distance in the RP phase Sr_2TiO_4.[44,45] Alkali and proton-containing layered perovskite-type metal oxides, including RP and the Dion-Jacobson phase, exhibit very interesting soft-chemical properties.[46−48] Accordingly, our future work will be directed to the substitution of alkali ions and protons and the trivalent cation for Sr in Sr_2CeO_4, which is likely to show similar technologically relevant chemical and physical properties.

Figure 3 shows the PXRD patterns for the conversion of 10 mol % YSCO into the corresponding YCO, which can be expressed using the chemical reaction

$$Sr_2(Ce, Y)O_{4-\delta} \xrightarrow{2CO_2,\ 800\ ^\circ C} 2SrCO_3 + (Ce, Y)O_{2-\delta} \xrightarrow[-2SrCO_3]{\text{Dilute HCl}} (Ce, Y)O_{2-\delta} \quad (1)$$

The exposure to CO_2 at elevated temperatures shows a complex diffraction pattern due to the presence of $SrCO_3$[49−52] and the fluorite-type CeO_2 (Figure 3b).[26,36,38] The weight gain after the CO_2 reaction was found to be close to about 2 mol of CO_2 per formula of Sr_2CeO_4, which is consistent with proposed reaction 1. About 80% of CO_2 capture per ceramic gram of material was observed experimentally at 800 °C. This variation in the CO_2 capturing value may be attributed to the desorption of CO_2 and also may be due to potential decomposition of the carbonates at elevated temperatures. It is also mentioned here that the CO_2 capturing ability of these materials was found to vary with the amount of the YSCO compound placed into the CO_2 reactor and with the temperature of the reaction. Samples were reheated in CO_2 to ensure the completion of decomposition reaction 1. Interestingly, the PXRD study of the acid-washed sample shows a single-phase fluorite-type structure with a cell constant of 5.412(1) Å for the $x = 1$ member of YCO (Figure 3c). The formation of 20 mol % Y_2O_3-doped CeO_2 from the corresponding YSCO is shown in Figure 4 ($a = 5.400(3)$ Å for the acid-washed sample for $x = 0.2$ member).

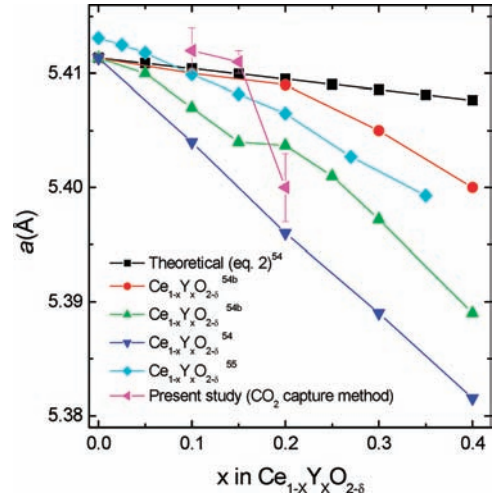

Figure 5. Comparison of the experimental lattice constants of Y_2O_3-doped CeO_2 with theoretical lattice parameter calculated using eq 2.[54] The observed lattice constant falls within the range reported for the same composition prepared by ceramic or soft-chemical methods.[54,55]

Figure 5 shows the theoretical lattice constant for $Ce_{1-x}Y_xO_{2-\delta}$ (CYO) together with the literature data.[54,55] The

(46) Gopalakrishnan, J. *Chem. Mater.* **1995**, 1265–1275.
(47) Bhuvanesh, N. S. P.; Gopalakrishnan, J. *J. Mater. Chem.* **1997**, *7*, 2297–2306.
(48) Schaak, R. E.; Mallouk, T. E. *Chem. Mater.* **2002**, *14*, 1455–1471.
(49) Guth, U.; Barwisch, F.; Wulff, H.; Mobius, H. H. *Cryst. Res. Technol.* **1986**, *21*, 431–435.
(50) Cao, M.; Wu, X.; He, X.; Hu, C. *Langmuir* **2005**, *21*, 6093–6096.
(51) Yu, J.; Guo, H.; Cheng, B. *J. Solid State Chem.* **2006**, *179*, 800–803.
(52) Shi, L.; Du, F. *Mater. Lett.* **2007**, *61*, 3262–3264.

Table 1. Compound, Lattice Constant, and Electrical Properties of CYO Prepared Using CO_2 Capture Method

compound, cell constant	T (°C)	$\sigma_{(bulk)}$ (S/cm)	capacitance (F) × 10^{-10}
$Ce_{0.9}Y_{0.1}O_{1.95}$, 5.421(2) Å	248	3.30×10^{-6}	9.1
	281	1.04×10^{-5}	7.2
	308	1.61×10^{-5}	6.83
	328	3.09×10^{-5}	8.2
	351	9.10×10^{-5}	9.95
	377	1.73×10^{-4}	4.77
	411	2.85×10^{-4}	1.9
$Ce_{0.8}Y_{0.2}O_{1.9}$, 5.411(2) Å	250	1.14×10^{-5}	7.87
	304	6.17×10^{-5}	8.41
	308	6.98×10^{-5}	7.66
	350	2.31×10^{-4}	7.9
	356	3.25×10^{-4}	7.02
	400	6.67×10^{-4}	9.1

expected lattice constant was calculated according to the following equation:[54]

$$a = \frac{4}{\sqrt{3}}[xr_{Y^{3+}_{(CN8)}} + (1-x)r_{Ce^{4+}_{(CN8)}} + (1-0.25x)r_{O^{x}_{o}} + 0.25xr_{V^{\bullet\bullet}_{o}}] \times 0.9971 \quad (2)$$

where x is the Y content ($0 \le x \le 0.4$) in $Ce_{1-x}Y_xO_{2-\delta}$. The ionic radius values were taken from the literature, where the Y^+ ionic size is $r_{Y^{3+}_{(CN8)}} = 1.02$ Å, the Ce^{4+} ionic size is ($r_{Ce^{4+}_{(CN8)}}$) = 0.97 Å, the O^{2-} ionic size is ($r_{O^{x}_{o}}$) = 1.38 Å, and the oxygen vacancy radius is ($r_{V^{\bullet\bullet}_{o}}$) = 1.164 Å.[54b] Expression 2 was developed originally by Hong and Virkar[54a] to compute the lattice constant of several metal-ion-doped CeO_2's. The theoretical lattice constant was found to slightly decrease with increasing Y content in YCO.[54] Taking Shannon's ionic radii into consideration (the ionic radius for 8-fold oxygen-coordinated Ce^{4+} ion is 0.97 Å; Y^{3+} is 1.02 Å),[53] one would envisage that the lattice constant should increase with increasing Y content in YCO. But, an opposite trend was observed which may be attributed to the formation of oxide ion vacancies.[54] Also, the lattice constant obtained for YCO prepared from Sr_2CeO_4 was found to be consistent with the literature trend (Figure 5).[54,55] The lattice parameter of the sintered (at 1350 °C) samples showed a slight increase (~0.01 Å) in the lattice constant (Table 1 and Figures 3d and 4d).

The EDX analysis confirms further conversion of the layered structured 10 mol % Y_2O_3-doped Sr_2CeO_4 compound into the corresponding YCO (Figure 6). EDX clearly shows the absence of Sr in the CO_2-treated and subsequent acid-washed (Figure 6b) and sintered (Figure 6c) samples. Similar EDX data were observed for the $x = 0.2$ member sintered sample (Figure 6d). The relative intensity due to Ce and Y was also found to be vary in the $x = 0.1$ and 0.2 members of CYO. The transformation of layered-structured Sr_2CeO_4 into fluorite-type CeO_2 is shown schematically in Figure 7. It must be mentioned that we have recently shown the preparation of fast oxide-ion-conducting Y-, Sm-, Sm+Ca-, and In-doped CeO_2 from the corresponding three-dimensional Ba-containing perovskite-like structure employing the CO_2 capturing method.[36,38] In the present work, we have used the two-dimensional layered-structured YSCO as a precursor to prepare fast oxide-ion-conducting YCO. Furthermore, the lattice constant of YCO falls within the range reported for Y_2O_3-doped CeO_2 prepared by other methods (Figure 5), suggesting that the Y_2O_3-doped fluorite compound can be obtained just by the CO_2 reaction at elevated temperatures.[54,55] We speculate that one could prepare novel fluorite-type structure materials by designing appropriate precursor compounds that are reactive in CO_2 and form carbonate at elevated temperatures.

The SEM investigation on powdered samples was carried out to understand the particle size distributions as well as the morphology. Figures 8 and 9 show typical SEM images corresponding to the PXRD results shown in Figures 3 and 4, respectively. A distinct difference was found in the particle size and morphology of the as-prepared precursor, CO_2-treated, acid-washed product, and the sintered samples. Doped Sr_2CeO_4 precursor samples showed large-sized particles compared to those of CO_2 treated materials. As expected, the CO_2-reacted and subsequent acid-washed product shows much smaller-sized particles. The sintered fluorite compounds show a significant growth in the particle size, which may be due to particle growth at elevated temperatures. This observation is consistent with our previous study.[36]

Electrical Conductivity. AC impedance studies on CO_2-capture-prepared YCO were found to be similar to those of materials synthesized by other methods. A bulk, grain boundary and electrode contributions in the frequency range of 10^{-2} to 10^7 Hz were observed. Figure 10 shows typical AC impedance plots of 10 and 20 mol % YCO obtained in the air. These impedance plots were highly reproducible during the heating and cooling runs. Similar AC impedance plots were reported for the present CO_2-capture- and ceramic-method-synthesized doped CeO_2.[26,36,38] A clear intercept or minimum due to bulk contributions in the high-frequency range was observed, especially at low temperatures (~200−450 °C). The capacitance value obtained from the high-frequency are using the relationship $\omega RC = 1$ (where $\omega = 2\pi f$, f is the frequency, and R is the resistance) was found to be in the range of 10^{-10} F values at the temperature range 250−400 °C (Table 1). This value is typical of the bulk contribution to the ionic conduction.[56,57] We observed a large overlap between the grain-boundary and electrode effects at low frequencies over the investigated temperature range (Figure 10). Hence, we are unable to meaningfully separate the bulk, grain-boundary, and electrode contributions over the entire temperature range of investigation. Thus, we have uniformly taken the bulk resistance from the high-frequency minimum/intercept along the Z′ axis of the impedance plots to calculate the electrical conductivity data.

Figure 11 shows the Arrhenius plot for the bulk ionic conductivity of CO_2-capture-method-prepared YCO in the

(53) Shannon, R. D. *Acta Crystallogr.* **1976**, *A32*, 751–767.
(54) (a) Hong, S. J.; Virkar, A. *J. Am. Ceram. Soc.* **1995**, *78*, 433–439. (b) Zhang, T. S.; Ma, J.; Huang, H. T.; Hing, P.; Xia, Z. T.; Chan, S. H.; Kilner, J. A. *Solid State Sci.* **2005**, *5*, 1505–1511.
(55) Li, J. G.; Ikegami, T.; Wang, Y.; Mori, T. *J. Solid State Chem.* **2002**, *168*, 52–59.
(56) Bauerle, J. E. *J. Phys. Chem. Solids* **1969**, *30*, 2657–2670.
(57) (a) Irvine, J. T. S.; Sinclair, D. C.; West, A. R. *Adv. Mater.* **1990**, *2*, 132–138. (b) Zhao, H.; Feng, S. *Chem. Mater.* **1999**, *11*, 958–964. (c) Losilla, E.; Aranda, M. A. G.; Bruque, S.; Sanz, J.; Paris, M. A.; Campo, J.; West, A. R. *Chem. Mater.* **2000**, *12*, 2134–2142.

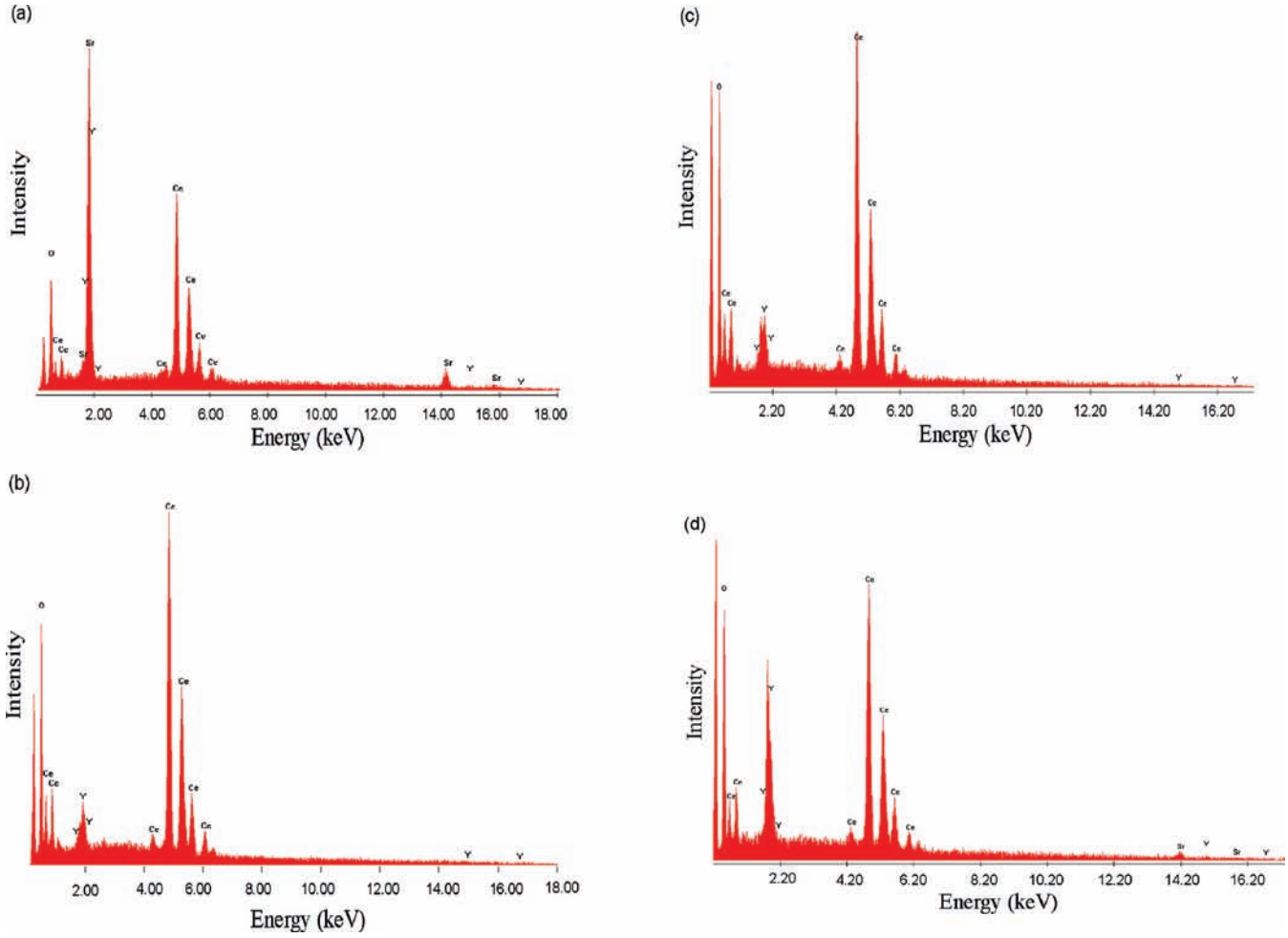

Figure 6. Energy dispersive X-ray analysis (EDX) of (a) as-prepared $Sr_2Ce_{0.9}Y_{0.1}O_{3.95}$, (b) sample "a" heated at 800 °C in CO_2 for 12 h and washed with dilute acid and dried in ambient air, and (c) sample "b" sintered at 1350 °C for 24 h in the air. In d, we show the EDX data of the $Ce_{0.8}Y_{0.2}O_{1.9}$ sintered sample.

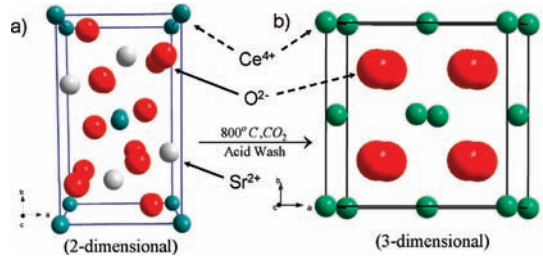

Figure 7. A schematic representation showing the transformation of (a) Sr_2CeO_4 into (b) fluorite-type structure CeO_2 under CO_2 reaction at an elevated temperature.

present work. The electrical conductivity data obtained during the first cycle heating and cooling and subsequent runs follow the same line, suggesting the equilibrium behavior of the sample. Very interestingly, the electrical conductivity of CO_2-capture-method-prepared doped samples was found to be about one and half orders of magnitude higher than that of undoped CeO_2. The bulk ionic conductivity of the $x = 0.2$ member was found to be slightly higher than that of the $x = 0.1$ member. The activation energy for the electrical conductivity was found to be 0.88 eV for the $x = 0.1$ member and 0.82 eV for the $x = 0.2$ member of CYO, which is comparable to that of the RE-doped CeO_2 reported in the literature.[27,58−61]

Typical impedance plots obtained for 20 mol % Y_2O_3-doped CeO_2 at 700 and 800 °C in three different atmospheres are shown in Figure 12. As expected, the bulk resistance (high-frequency intercept) of doped YCO was found to be the same in the investigated temperature range of 600−800 °C in the air, N_2, and Ar. The electrode contribution was found to increase with decreasing oxygen partial pressures. Figure 13 compares the bulk ionic conductivity data of $Ce_{0.8}Y_{0.2}O_{1.9}$ with that of the doped CeO_2 reported in the literature.[15] The electrical conductivity data of the presently prepared CO_2-capture-method YCO exhibit comparable electrical conductivity values to those in the literature,[15] especially at low temperatures (≤ 600 °C).

Conclusions

The present study deals with the preparation of novel fluorite-type structure materials by designing appropriate precursor compounds that are reactive in CO_2. We have

(58) Mogensen, M.; Sammes, N.; Tompsett, G. *Solid State Ionics* **2000**, *129*, 63–94.
(59) Huang, W.; Shuk, P.; Greenblatt, M. *Solid State Ionics* **1997**, *100*, 23–27.
(60) Huang, W.; Shuk, P.; Greenblatt, M. *Chem. Mater.* **1997**, *9*, 2240–2245.
(61) Huang, K.; Feng, M.; Goodenough, J. B. *J. Am. Ceram. Soc.* **1998**, *81*, 357–362.

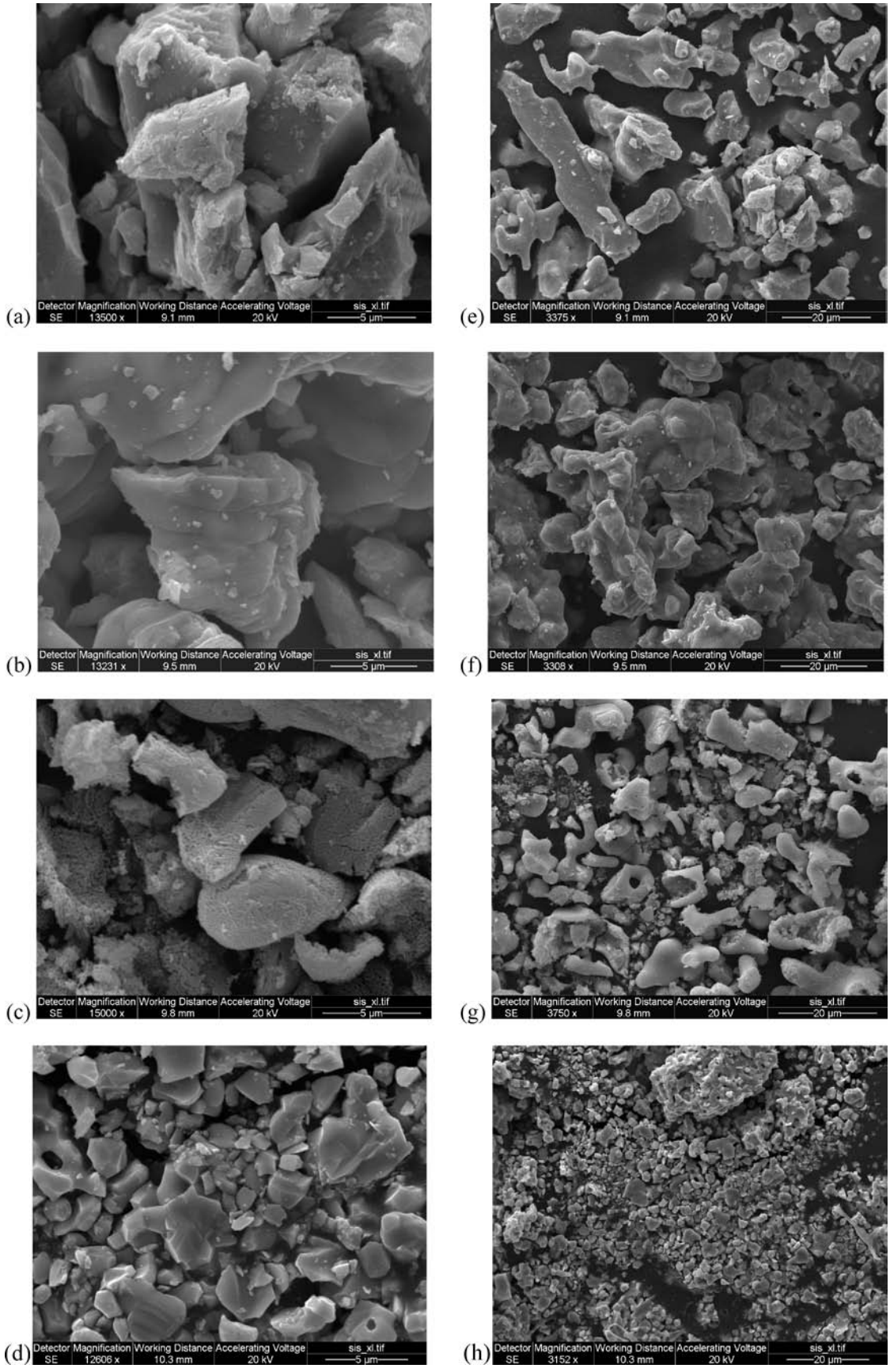

Figure 8. Scanning electron microscopy (SEM) images of (a) as-prepared $Sr_2Ce_{0.9}Y_{0.1}O_{3.95}$, (b) sample "a" heated to 800 °C in CO_2 for 12 h, (c) sample "b" washed with dilute acid and subsequently dried in ambient air, and (d) sample "c" sintered at 1350 °C for 24 h in the air. The left-hand side shows the diagram at 5 μm, and the right-hand side shows the corresponding samples ((e)–(h)) at a higher scale, 20 μm.

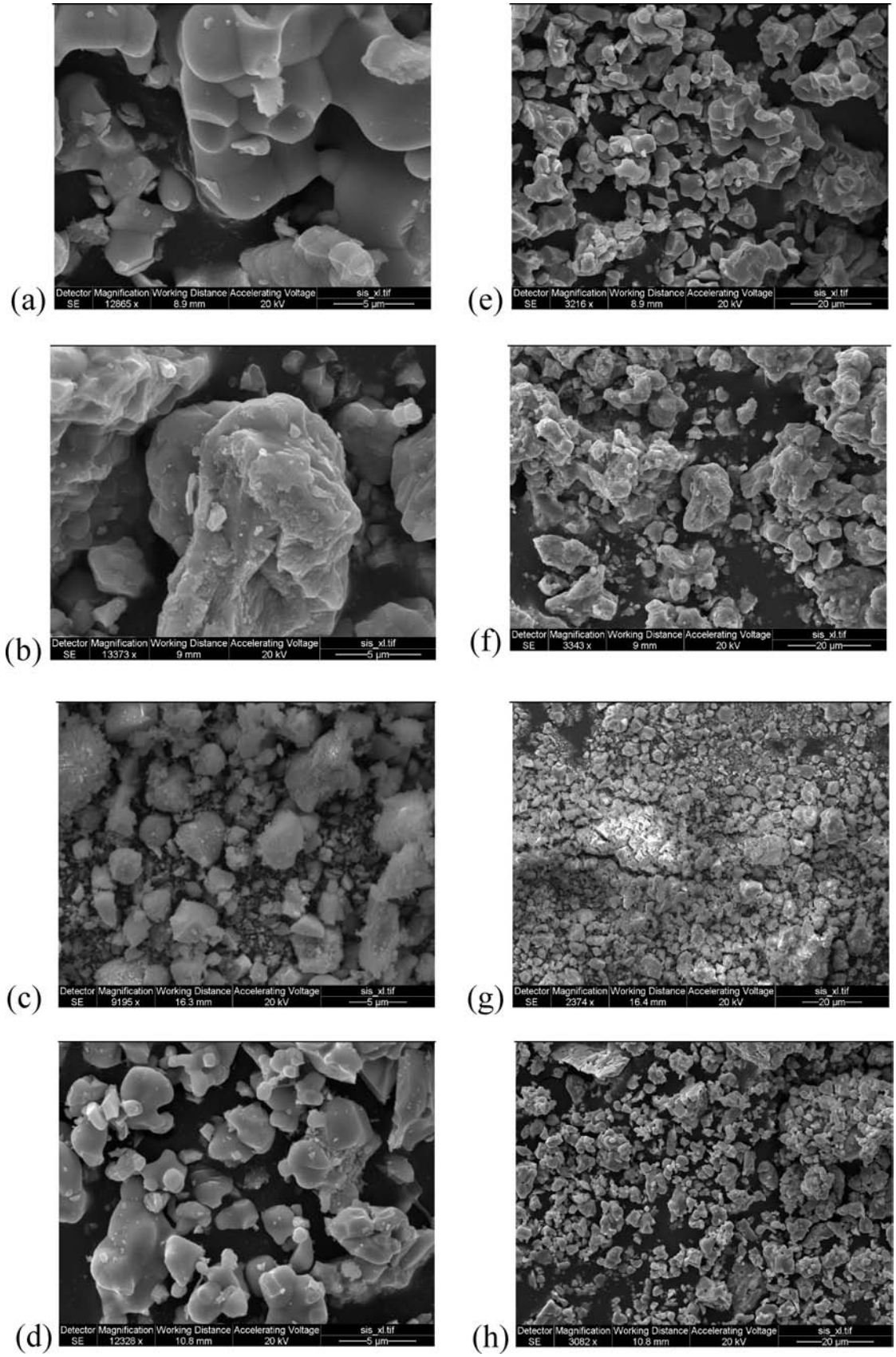

Figure 9. Scanning electron microscopy (SEM) images of (a) as-prepared $Sr_2Ce_{0.8}Y_{0.2}O_{3.9}$, (b) sample "a" heated to 800 °C in CO_2 for 12 h, (c) sample "b" washed with dilute acid and subsequently dried in ambient air, and (d) sample "c" sintered at 1350 °C for 24 h in the air. The left-hand side shows the diagram at 5 μm, the and right-hand side shows the corresponding samples ((e)–(h)) at a higher scale, 20 μm.

shown the formation of Y_2O_3-doped CeO_2 (YCO) from the corresponding Y_2O_3-doped layered-structured Sr_2CeO_4 and CO_2 at 800 °C and subsequent to acid washing. The amount of CO_2 gained was found to be consistent with 2

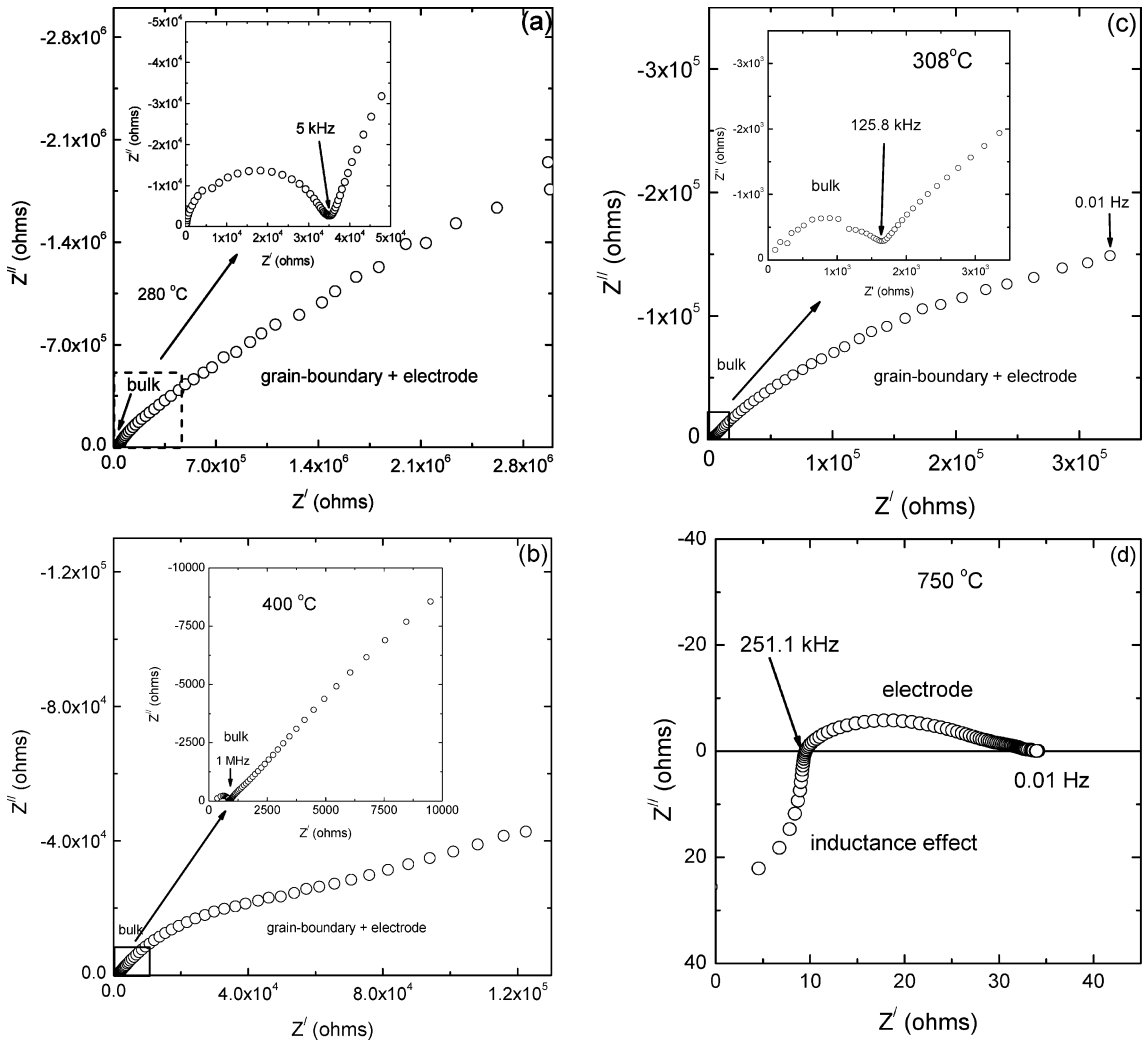

Figure 10. AC impedance plots of CO_2 capture method synthesized $Ce_{0.9}Y_{0.1}O_{1.95}$ at (a) 280 °C and (b) 400 °C in the air. Parts c and d show the ac impedance data for $Ce_{0.8}Y_{0.2}O_{1.9}$ at 308 and 750 °C in the air, respectively. Insets in a−c show the expanded view.

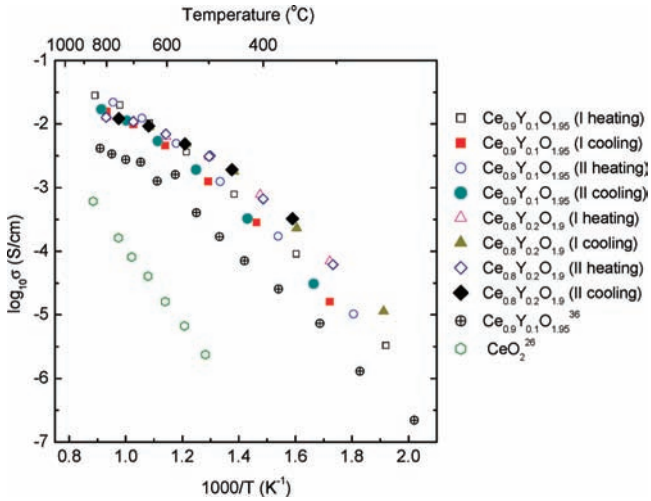

Figure 11. Arrhenius plots for the electrical conductivity of $Ce_{0.9}Y_{0.1}O_{1.95}$ and $Ce_{0.8}Y_{0.2}O_{1.9}$ prepared by the CO_2 capturing method. For comparison, the electrical conductivities of parent CeO_2[26] and 10 mol % Y-doped CYO[36] are included.

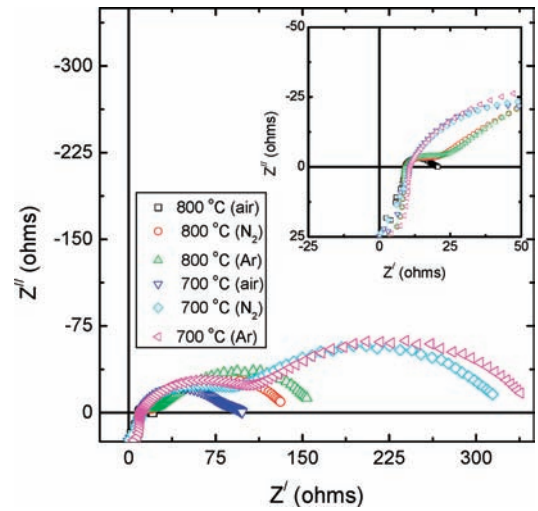

Figure 12. AC impedance plots of CO_2 capture method synthesized $Ce_{0.8}Y_{0.2}O_{1.9}$ at 700 and 800 °C in the air and N_2 and Ar in the frequency range 10^{-2} to 10^7 Hz. Inset shows the expanded view.

mol of CO_2 per formula unit of the layered structure cerates. The PXRD investigations show that the lattice parameter decreases with increasing temperature, which is expected on the basis of the ionic radii trend. Also, the lattice constant value was found to be comparable to that of ceramic- and chemical-method-synthesized YCO. EDX investigations further confirmed the PXRD results. The SEM characterization reveals much smaller-sized particles

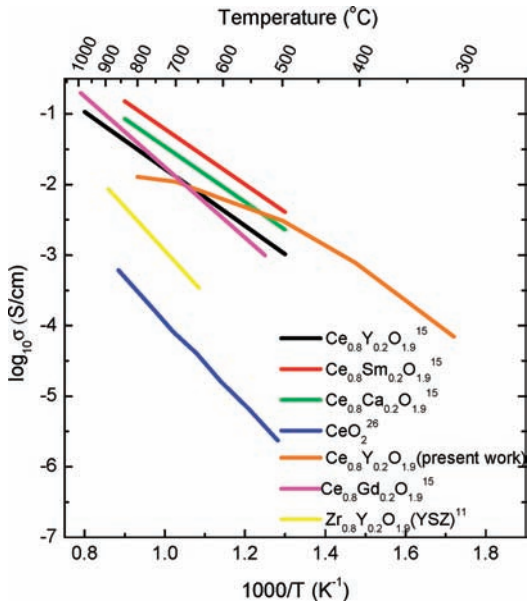

Figure 13. Comparison of the electrical conductivity of $Ce_{0.8}Y_{0.2}O_{1.9}$ prepared by CO_2 capture method using $Sr_2Ce_{0.8}Y_{0.2}O_{3.9}$ with the conventional YSZ,[11] parent CeO_2,[26] and rare-earth-doped CeO_2[15] reported in the literature.

for the CO_2-treated and acid-washed samples compared to the precursor and sintered product. The capacitance value determined using the high-frequency part was found to be on the order of 10^{-10} F. The bulk ionic conductivity of CO_2-capture-method-prepared YCO exhibits about one and half orders higher electrical conductivity than that of the undoped CeO_2. The activation energy for bulk ionic conductivity of YCO was found to be comparable to those of ceramic-method-prepared YCO samples with a similar chemical composition.

Acknowledgment. This research was supported partially by funding to the NSERC Solid Oxide Fuel Cells Canada Strategic Research Network and the Discovery Grants from the Natural Science and Engineering Research Council (NSERC). We also would like to thank the Canada Foundation for Innovation (CFI) for support through the Leaders Opportunity Fund (LOF) funding.

IC801729X